Turkish Journal of Electrical Engineering & Computer Sciences

http://journals.tubitak.gov.tr/elektrik/

Research Article

Turk J Elec Eng & Comp Sci
(2024) 32: 285 – 304
© TÜBİTAK
doi:10.55730/1300-0632.4069

Cascade controller design via controller synthesis for load frequency control of electrical power systems

Yavuz GÜLER[1], **Mustafa NALBANTOĞLU**[2], **İbrahim KAYA**[3*]
[1]Department of Electronics and Automation, Technical Sciences Vocational School, Muş Alparslan University, Muş, Turkiye
[2]Department of Electrical and Electronics Engineering, Faculty of Engineering and Architecture, Kilis 7 Aralık University, Kilis, Turkiye
[3]Department of Electrical and Electronics Engineering, Faculty of Engineering, Dicle University, Diyarbakır, Turkiye

Received: 29.10.2023 • **Accepted/Published Online:** 17.02.2024 • **Final Version:** 14.03.2024

Abstract: The regulation of tie-line electricity flow and frequency of electrical power systems (EPS) is crucial for ensuring their robustness to parameter changes and efficient management of disturbances. To this end, a novel cascade control design approach utilizing a serial Proportional-Integral-Derivative controller with a filter (PIDF) is proposed in this paper. The parameters of the controllers are derived analytically, and it is employed in both loops of the cascade control system to regulate the Load Frequency Control (LFC) of EPS. The implementation of PIDF controllers in both loops is utilized in the cascade control scheme for various power systems featuring different turbine topologies. This approach has been applied to single, and two-area power systems and has exhibited enhanced performance compared to other commonly referenced studies in the literature. To assess the effectiveness of the cascade control approach proposed performance metrics such as settling time, peak value (overshoot), and integral absolute error (IAE) value of frequency and tie-line power variations are utilized to gauge the system's response to a load perturbation. Additionally, the suggested cascade control technique and design process have undergone robustness testing with ±50% changes in system parameters to validate their reliability.

Key words: Load frequency control, PIDF, cascade control, controller synthesis

1. Introduction

The demand for a high-quality electrical power source is continuously rising in today's technology. Consequently, the production of electric power is crucial for electrical systems [1]. Field frequencies and tie-line power (TLP) variation may fluctuate due to the complicated structure of power systems (PS). To maintain the stability of a PS, there must be synchronization between the generation, transmission, and distribution of power within the PS. The load frequency control (LFC), which guarantees the synchronization and reliability of the PS [2], is critical. Power system reliability is achieved in contemporary power systems through the use of properly designed controllers. Thus, selecting the appropriate controller type and design approach are key components of a successful LFC controller design [3].

Numerous LFC systems are consistently researched utilizing various controllers. Dash et al. [4] employed the Flower Pollination Algorithm (FPA) to optimize the parameters of their PI-PD cascade controller design

*Correspondence: ikaya@dicle.edu.tr

This work is licensed under a Creative Commons Attribution 4.0 International License.

technique for the LFC of a four-area power system. The suggested design technique has disadvantages such as extended settling time, high peak values, and oscillating output values. Padhy and Panda [5] introduced a cascade PI-PD controller based on a hybrid Stochastic Fractal Search plus Pattern Search (hSFS-PS) for LFC of PS comprised of gas, hydro, and thermal power units, including Plug-in Electric Vehicles (PEV). The suggested approach has a high settling time in response to load variations. Saxena [6] suggested a fractional order proportional-integral-derivative (FOPID) controller design using internal model control (IMC) for the LFC of hydro, reheated, and nonreheated turbines, resulting in lower performance metrics than earlier design methodologies. For the LFC problem of single/multiarea reheated thermal and hydrothermal PS, Sonker et al. [7] suggested a dual loop-IMC (DL-IMC) method. Çelik et al. [8] suggested the LFC for a single/two-area and multi-source PS with (1+PD)-PID Cascade control (CC). The gains were adjusted using the Dragons Fly Search algorithm (DSA). However, large peak values offer a challenge for the suggested design strategy. Kumar et al. [9] presented the sliding mode controller method for the LFC of single/two-area PS, where the controller parameters were determined by the grey wolf and particle swarm optimization methods. In another work by Kumar et al., [10], a 2Dof-PID control strategy was developed using the Direct Synthesis (DS) technique for the LFC of a single/multiarea PS composed of various turbines. Saka et al. [11] proposed PI controller design using optimization techniques for LFC of multiarea power systems with communication time delay. Guler and Kaya [3] proposed a PI-PD control design strategy based on the weighted geometric center method to address frequency oscillation in a single-area single/multi-source PS consisting of various hydro, gas, nonreheat, and reheat thermal turbine units. Barakat et al. [12] introduced a new cascade controller (CC) consisting of a PIDn controller and a proportional-integral (PI) controller for the LFC of a two-area PS composed of a photovoltaic and a reheated thermal unit. However, the suggested approach has the problem of producing extremely high peak values in the output. Abou El-Ela et al. [13] suggested an optimum coyote optimization algorithm-based cascade proportional derivative with filter-proportional integral (PDn-PI) controller design. The responses of the proposed control system appear to have long settling times and noticeable oscillations. To compensate for frequency and TLP variations in single/multiarea PS incorporating energy storage devices (ESD), such as a redox flow battery (RFB) and superconducting magnetic energy storage, Choudhary et al. [14] suggested a CC consisting of a FOPI-FOPTID controller. The suggested design technique has significant settling periods and oscillations due to changes in power system parameter values. Khokhar et al. [15] developed a FOPID+DD controller using a water wave optimization approach for LFC in hybrid power systems. Çelik [16] developed the fuzzy 1+ proportional + derivative (F1PD)-PI controller to automate production control in an interconnected power system using renewable energy sources. Khokhar et al. [17] proposed a recently developed Salp Swarm Optimization (SSO) algorithm-based PI-PD CC for LFC in standalone microgrids with energy storage systems and electric vehicles. Furthermore, Khokhar et al. [18] developed an FPD-TID controller for the LFC of standalone microgrids.

When designing a controller, it is necessary to choose an appropriate control method for the LFC of PS. The control approach should withstand load disturbances and changes in power system parameters [3]. The cascade control approach is known for its robustness against parameter uncertainty and severe load disturbances [19, 20]. If a system can be separated into two subsequent systems, the CC technique may be used to control it. However, if it cannot be decomposed into two different sequential systems, the CC approach cannot be used, indicating a significant restriction of the method. Therefore, in this study, the cascade control structure is preferred to suppress parameter changes and load disturbances in power systems, aiming to achieve superior performance

in terms of the least settling time, the least peak value, etc. Notably, this study introduces a crucial feature, wherein analytical expressions are utilized to design the parameters of both the internal and external controllers in the cascade control system. The adoption of analytical expressions for designing these controllers not only ensures improved accuracy but also enables precise tuning to meet specific control requirements. Overall, this feature highlights the significance of analytical expressions in enhancing the performance of the cascade control system. The technique of controller synthesis was employed to assess the appropriate controller structures, which were determined to be serial PID controllers with a filter (PIDF) for both loops. The proposed CC design methodology was initially applied to a single-area power system with reheated and nonreheated turbines. Subsequently, the same CC design technique was implemented in two-area power systems. The results demonstrate that the proposed CC design methodology effectively ensures the stability of power systems by regulating their frequency. The efficacy and robustness of the suggested CC system are assessed by accounting for a variation of up to $\pm 50\%$ in plant transfer function values at varying intervals. Simulations show that the suggested CC design technique for LFC exceeds previously introduced methods in terms of efficiency and robustness. The evaluation was conducted in both single and two-area PS, based on performance evaluation criteria such as settling time, peak value (overshoot), and integral of absolute error (IAE) of change in frequency or tie-line power exchange (TLPE).

The following is a summary of this paper's major contributions:

i. This paper introduces a unique PIDF-PIDF cascade control approach as a solution for addressing the frequency and TLP deviations in single or two-area power systems. This innovative technique demonstrates high efficiency and accuracy in correcting such deviations, making it a valuable addition to the field of power system control.

ii. Unlike previous studies that employed various optimization approaches for cascade control designs in LFC of power systems, this research provides an analytical solution for identifying controller parameter values in the CC design technique. This contribution is significant and holds the potential for improving control performance and system stability.

iii. The suggested CC technique for single/two-area power systems with diverse turbines exhibits high robustness and effectiveness in managing uncertain system characteristics and unpredictable load patterns. The recommended CC strategy for LFC outperforms recently established solutions, resulting in significant performance improvements and enhanced system resilience.

The sections of this paper are as follows: Models of power systems are described in Section 2. The suggested controller synthesis-based cascade control design for LFC is presented in Section 3. Section 4 presents the findings of the simulation, and Section 5 concludes the findings of the study.

2. Description of power system model

The EPS actually has nonlinear characteristics because of its complicated structure [21]. However, in the literature, linear models of power systems are commonly employed for LFC rather than utilizing their nonlinear formulations. When electrical systems are exposed to step load perturbation (SLP) or small load changes (SLC), the LFC plays a crucial role in regulating the frequency deviation [3]. This paper discusses one/two area LFC systems due to limited pages but it may be applied to three or more areas of LFC systems.

2.1. Single-area power system

Figure 1 illustrates the linear model of a single area PS. In this configuration, a single-area PS for LFC consists of a governor, a turbine, a load & machine, and drop characteristics. The PS incorporates both nonreheat

thermal and reheat thermal turbines, which are two distinct types of turbines [21]. $1/R$ represents the droop characteristic. The governor and load and machine transfer function models are, respectively, provided by:

$$G_G(s) = \frac{1}{1+T_g s} \tag{1}$$

$$G_P(s) = \frac{K_P}{1+T_P s} \tag{2}$$

In the equations above, T_g and T_P, denote the governor time constant and the electrical system time constant, respectively. The transfer function models for reheated and nonreheated thermal turbine dynamics are correspondingly given by:

$$G_{T,RT}(s) = \frac{1+cT_r s}{(1+T_T s)(1+T_r s)} \tag{3}$$

$$G_{T,NRT}(s) = \frac{1}{1+T_T s} \tag{4}$$

where T_T is the turbine time constant, and T_r is the reheated turbine's time constant. The system model used in LFC design in a single-area power system is given as follows:

$$G_{TR}(s) = \frac{\Delta f(s)}{u(s)} = \frac{G_P(s)G_G(s)G_T(s)}{1+G_P(s)G_G(s)G_T(s)/R} \tag{5}$$

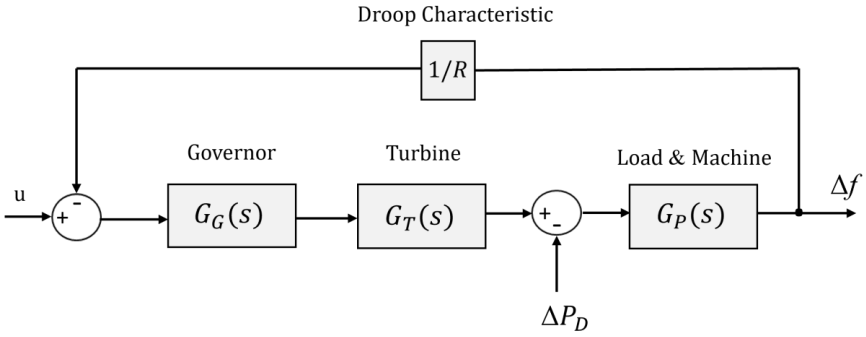

Figure 1. The linear model of a single-area PS [22].

2.2. Two-area power system

The LFC of a single-area PS can be expanded to two- or multiarea. A two-area PS model consisting of a nonreheat thermal turbine is given in Figure 2. Multiarea PS differs from single-area PS in that it is wanted to regulate both the TLPE and the frequency deviation as the load demand varies [23]. Frequency deviation in area-1, frequency deviation in area-2, and TLPE are denoted by Δf_1, Δf_2 and ΔP_{tie}, respectively. Area control error (ACE) is expressed as [24]:

$$ACE_i = B_i \Delta f_i \pm \Delta P_{tie} \tag{6}$$

where B_i is the frequency bias coefficient, Δf_i is the frequency deviation and ΔP_{tiei} is tie-line power exchange between the areas, as calculated by [24]:

$$\Delta P_{tie,i} = \sum_{j=1,i\neq j}^{N} \Delta P_{tie,ij} = \frac{1}{s}[\sum_{j=1,i\neq j}^{N} T_{ij}\Delta f_i - \sum_{j=1,i\neq j}^{N} T_{ij}\Delta f_j] \tag{7}$$

Here, T_{ij} is the synchronizing power constant. The control action of the i.th area can be given as follows:

$$u_i = -K_i(s)ACE_i \tag{8}$$

Since multiarea PS are assumed to have no TLPE ($\Delta P_{tie} = 0$) for LFC [23], the feedback in each area can be given as follows:

$$u_i = -K_i(s)B_i\Delta f_i \tag{9}$$

For each area, the decentralized controller may be tuned by multiplying the plant model with the local frequency bias coefficient (B_i). Therefore, the transfer function model of the i.th area may be stated as:

$$G_{TRi}(s) = B_i \frac{G_{Pi}(s)G_{Gi}(s)G_{Ti}(s)}{1+G_{Pi}(s)G_{Gi}(s)G_{Ti}(s)/R_i} \tag{10}$$

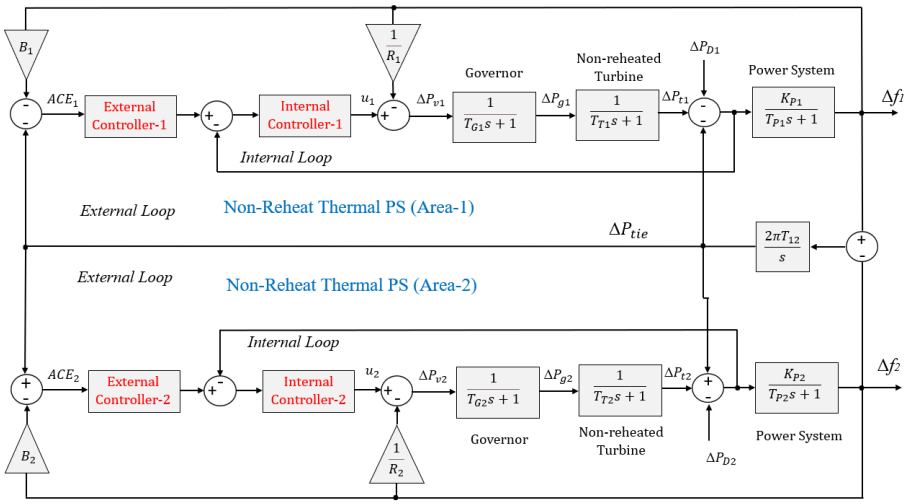

Figure 2. Power system model of two-area nonreheat thermal turbine with cascade control structure [19].

3. Cascade control design with controller synthesis approach

The concept of cascade control, as proposed by Franks and Worley [20], aims to enhance the performance of a control system under disturbances. If there is an extra measurement point, a CC method can successfully minimize disturbances [25]. The CC structure has two control loops, as illustrated in Figure 3. The process $G_{P2}(s)$ and a secondary controller $G_{C2}(s)$ are included in the internal loop, and the process $G_{P1}(s)$ and main controller $G_{C1}(s)$ are included in the external loop [26]. Here, it is presumed that the disturbance enters the control system as an input load disturbance, d_1, to $G_{P1}(s)$, as shown in Figure 3. It should be noted that d_1 in Figure 3 corresponds to ΔP_D in Figure 1. The outputs of the internal and external control loop are Y_2 and

Y_1, respectively. It needs to be pointed out that Y_2 and Y_1 in Figure 3 are equivalent to the input point of the power system or load & machine and Δf in Figure 1, respectively. In addition to the primary controller, a secondary measuring point and secondary controller are used to enhance the system's dynamic response to load variations in the power system [27].

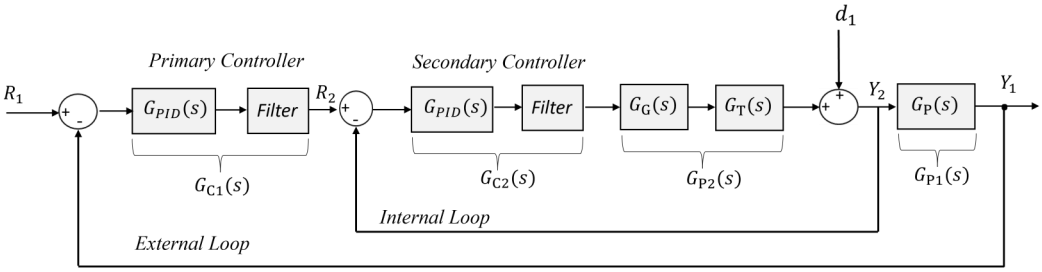

Figure 3. Cascade control structure.

3.1. Controller synthesis design method

The controller synthesis design technique introduced in [28] has been adopted in the present study to determine the internal and external loop controller parameter values of the CC. In this research, it is assumed that the external loop plant can be modelled by a first-order while the internal loop plant can be modelled by a third-order transfer function. It is important to highlight that the controller synthesis design may be applied to higher-order plant transfer function models in two ways. First, the high-order plant transfer function itself may be utilized to derive the appropriate equations. However, this strategy is rarely used since it results in computing complexity and high-order controllers, which are not desirable. Instead, high-order plant transfer functions are described as low-order plant transfer function models, and the design is carried out using this low-order model. Here, it would be useful to clarify that a power system is also often distinguished by complicated nonlinear large-scale systems [1]. However, for the problem of load frequency control, the system can be linearized around its operational point. Almost the majority of the research in the literature has employed this strategy [6, 35]. This simplifies the controller design and reduces computing complexity. As shown in Figure 3, the internal loop closed-loop transfer function can be seen to be given by:

$$\frac{Y_2(s)}{R_2(s)} = \frac{G_{P2}(s)G_{C2}(s)}{1+G_{P2}(s)G_{C2}(s)} \tag{11}$$

The following can be identified by solving (11) for the internal loop controller:

$$G_{C2}(s) = \frac{1}{G_{P2}(s)} \frac{Y_2(s)/R_2(s)}{1-Y_2(s)/R_2(s)} \tag{12}$$

As is seen from (12), the internal loop plant transfer function, $G_{P2}(s)$, and the desired internal closed-loop transfer function, $Y_2(s)/R_2(s)$, are required to identify the internal loop controller. In this case, it is supposed that the internal loop plant transfer function and the desired internal closed-loop transfer function are each provided by:

$$G_{P2}(s) = \frac{K_2(T_1 s+1)}{(T_2 s+1)(T_3 s+1)(\theta_2 s+1)} \tag{13}$$

$$\frac{Y_2(s)}{R_2(s)} = \frac{1}{(\tau_c s+1)} \tag{14}$$

where τ_c is the internal closed-loop time constant. By substituting the terms in (13) and (14) into (12), the internal loop controller is readily identified:

$$G_{C2} = \frac{T_2}{K_2\tau_c}(1+\frac{1}{T_2 s})(1+\theta_2 s)[\frac{T_3 s+1}{T_1 s+1}] \tag{15}$$

The controller provided in (15) is a serial PID with a filter. The following are the PID controller parameters:

$$K_{ci} = \frac{T_2}{K_2\tau_c} \tag{16}$$

$$T_{ii} = T_2 \tag{17}$$

$$T_{di} = \theta_2 \tag{18}$$

It should be noted that the internal loop controller parameters given by (16), (17), and (18) are dependent on the time constant, τ_c, of the internal closed-loop transfer function and the internal loop process transfer function parameters, namely, K_2, T_2 and θ_2. Since it is assumed that the plant transfer function is known, it is simple to evaluate the internal loop controller settings once the internal closed-loop time constant, τ_c, has been selected. To design the external loop controller, it has been assumed that the external loop plant transfer function has to be:

$$G_{P1}(s) = \frac{K_1}{(T_4 s+1)} \tag{19}$$

As a result, for the cascade system shown in Figure 3, the complete open loop transfer function is provided by

$$G_t(s) = \frac{K_1}{(T_4 s+1)(\tau_c s+1)} \tag{20}$$

Since the CC system's open-loop transfer function is of second order, the following is supposed to be the desired external closed-loop transfer function:

$$\frac{Y_1(s)}{R_1(s)} = \frac{\omega_n^2}{s^2+2\xi\omega_n s+\omega_n^2} \tag{21}$$

In (21), ξ and ω_n are the damping ratio and natural frequency assigned by the user, respectively. The external loop controller can be determined by following the same method used in the internal loop. The terms in (20) and (21) were inserted into (12) with $Y_2(s)/R_2(s)$ and $G_{P2}(s)$ replaced by $Y_1(s)R_1(s)$ and $G_t(s)$, respectively:

$$G_{C1} = \frac{\omega_n T_4}{K_1(2\xi)}(1+\frac{1}{T_4 s})(1+\tau_c s)[\frac{1}{as+1}] \tag{22}$$

The external loop controller described in (22) is also a serial PID controller with a filter, just like the internal loop instance. The constants of filter transfer function, a as well as PID controller tuning parameters, K_c, T_i, and T_d, are provided below:

$$a = \frac{1}{2\xi\omega_n} \tag{23}$$

$$K_{co} = \frac{\omega_n T_4}{2\xi K_1} \tag{24}$$

$$T_{io} = T_4 \tag{25}$$

$$T_{do} = \tau_c \tag{26}$$

The external loop plant transfer function parameters, natural frequency, and user-specified damping ratio affect the values of the external loop controller parameters provided in (24), (25), and (26). Assuming that the external loop plant transfer function is known, the damping ratio and natural frequency values should be chosen in order to assess the external loop controller settings. Since it is well known that a closed-loop response will typically be well-damped when the damping ratio is between 0.7 and 1.0. It might not be so simple to decide on the natural frequency, though. Therefore, the following equation [29] may be useful in determining the most optimal natural frequency value:

$$\omega_n = \frac{4.5}{\xi T_s} \tag{27}$$

In (27), T_s is the user-defined settling time. As a result, if appropriate values of the external loop's settling time, τ_c, and the internal loop's closed-loop time constant, τ_c, are chosen, then (16)-(18) can be used to calculate the internal loop PID controller settings and (24)-(26) can be used to calculate the PID controller settings for the external loop. In this research, $T_s = 0.5s$ is specified for all simulation cases. The following relationship is suggested for choosing a suitable value of τ_c:

$$\tau_c = \frac{T_s}{n} \tag{28}$$

where, n is an integer with a range of 5 to 25. Different methods can be used to find the optimal value of n. The IAE is to be used in this case. To accomplish this, the minimal value of IAE will be explored for various values of ξ and n. The following equations are used to estimate the minimal value of IAE for a single and multiarea PS in order to decide on ξ and n values that will be utilized for assessing the suggested CC controller parameters:

$$IAE = \int_0^T |\Delta f| dt \tag{29}$$

$$IAE = \int_0^T [|\Delta f_i| + |\Delta P_{tiei-j}|] dt \tag{30}$$

where i=area number (1,2,3,4), $j = 1, 2, 3, 4$ $(i \neq j)$

4. Simulation results

This section presents a range of case examples, which highlight the superiority of the recommended CC scheme and the design method. These examples involve single and/or multiarea power systems that use various turbines. The purpose of these examples is to demonstrate how the suggested CC scheme and design approach offer a more efficient and cost-effective solution for power generation. By analyzing these case examples, we can observe the benefits of implementing the recommended CC scheme and design process in different scenarios.

4.1. Case 1: LFC design of single-area PS with nonreheat thermal turbine

The linear model of a single-area PS with nonreheat thermal turbine is shown in Figure 1. The nominal parameter values of the single-area PS are taken as $T_G = 0.08$, $T_T = 0.3$, $K_P = 120$, $T_P = 20$, and $R = 2.4$ [30]. The internal loop plant transfer function, $G_{P2}(s)$, constitute of transfer functions of the governor, $G_G(s)$, and nonreheat thermal turbine, $G_{T,NRT}(s)$. Therefore, it is given by:

$$G_{P2}(s) = G_G(s) G_{T,NRT}(s) = \frac{1}{(0.3s+1)(0.08s+1)} \tag{31}$$

In section 3.1, while designing the internal loop controller, the internal loop model transfer function was supposed to be provided by (13). Now, comparing (13) and (31), the internal loop's model transfer function parameters

are seen to be given by $K_2 = 1$, $T_1 = 0$, $T_2 = 0.3$, $T_3 = 0$ and $\theta_2 = 0.08$. To find the internal loop PID controller parameters from (16)-(18), one must first determine the internal loop closed loop time constant, τ_c, which relies on n and T_s as shown in (28). As a consequence, values of n and T_s should be identified first. $T_s = 0.5s$ is chosen throughout the article, as mentioned previously. The lowest IAE value in (29) is used to find the values of n and the damping ratio, ξ. Figure 4 depicts the IAE values as n and ξ are varied within defined limits. Accordingly, the lowest IAE value is achieved with $n = 24$ and $\xi = 0.4$ values. Thus, closed loop time constant is found to be $\tau_c = 0.02$, which then leads to $K_{ci} = 14.42$, $T_{ii} = 0.3$ and $T_{di} = 0.08$ using (16)-(18). Furthermore, it is found that $T_3 = 0$ and $T_1 = 0$ provide the internal loop PID controller filter constants. To design the external loop PID controller, one should notice that the external loop transfer function, $G_{P1}(s)$, is equal to the load & machine transfer function, $G_P(s)$, of the single-area PS, which is given below:

$$G_{P1}(s) = G_P(s) = \frac{120}{(20s+1)} \tag{32}$$

Therefore, the overall open loop transfer function of the CC configuration from (20) is given by:

$$G_t(s) = \frac{120}{(20s+1)(0.02s+1)} \tag{33}$$

Comparing (33) to (20) yields $K_1 = 120$ and $T_4 = 20$. It should be noted that $\tau_c = 0.02$, $n = 24$, and $\xi = 0.4$ were already determined during the internal loop PID controller design. Thus, natural frequency can be calculated to be $\omega_n = 22.5$ rad/s from (27). As a result, (23)-(26) are used to identify the external loop PID controller and filter parameters as $K_{co} = 4.69$, $T_{io} = 20$ and $T_{do} = 0.02$, and $a = 0.06$. Table 1 tabulates the internal and external loop controller parameters of the proposed CC approach. Table 1 also includes the controller parameters for the design techniques of Güler & Kaya [3], Saxena [6], Sondhi & Hote [22], Singh et al. [30], Kumar & Anwar [23], which will be used for comparison. Closed loop responses of all design methods to a step change in load ($\Delta P_D = 0.01 p.u.$) at $t = 1s$, are demonstrated in Figure 5a.

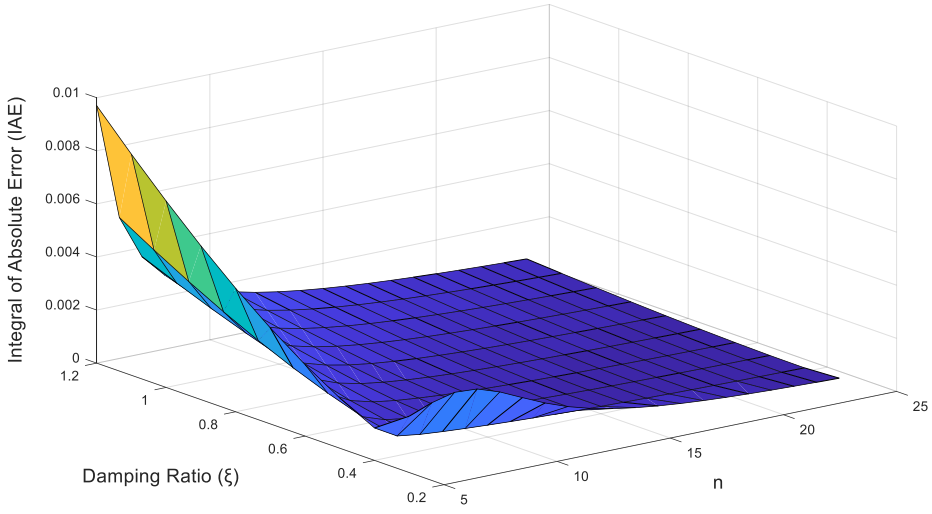

Figure 4. Integral of the absolute error (IAE) value of damping ratio (ξ) and n parameter values for Case 1.

It is observed that the proposed CC design method and design method of Güler & Kaya [3] result in very comparable results in terms of the least deviation and the shortest settling time. The suggested method, additionally, generates no oscillations and thus the smoothest response. Table 2 shows performance assessment indices such as settling time, peak value, and IAE for all design techniques under consideration. The previous observations are supported by the data in Table 2. The efficacy of all design methods is examined for +50% and -50% changes in the plant transfer function parameters, as shown in Figure 5b and Figure 5c. Table 2 shows the performance metrics for the aforementioned cases. As shown in the figures and Table 2, the suggested design strategy and design method of Güler & Kaya [3] establish the most desirable performances, similar to the nominal case. However, the suggested CC approach may be preferable in reality, since it produces smoother responses.

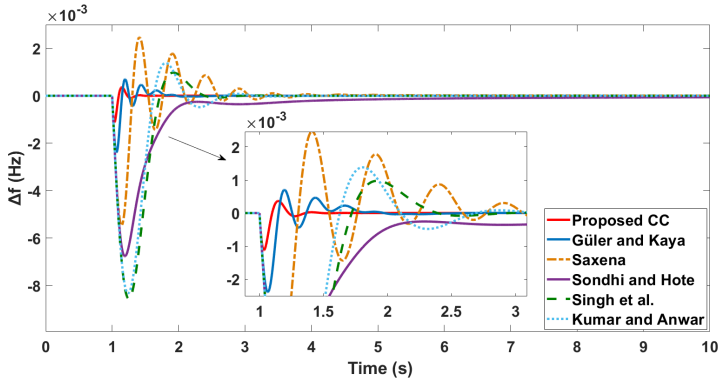

(a) Nominal parameters

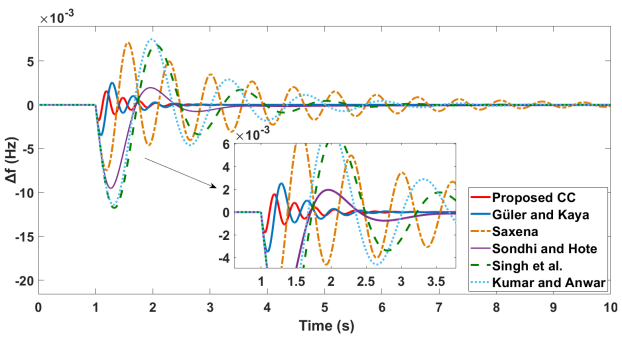

(b) +50% perturbations in plant transfer function parameters

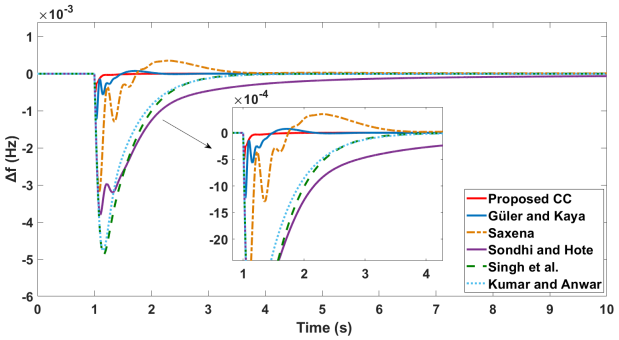

(c) -50% perturbations in plant transfer function parameters.

Figure 5. Frequency responses of system for case 1.

4.2. Case 2: LFC design of single-area PS with reheat thermal turbine

Let us consider a single-area PS with a reheat thermal turbine, which has nominal parameter values of $T_G = 0.08$, $T_T = 0.3$, $K_P = 120$, $T_P = 20$, $T_r = 4.2$, $c = 0.35$ and $R = 2.4$ [30]. Transfer functions of the governor, $G_G(s)$, and the reheated thermal turbine, $G_{R,RT}(s)$, constitute the internal loop plant transfer function, $G_{P2}(s)$, of the proposed CC method. Hence, $G_{P2}(s)$ is given by:

$$G_{P2}(s) = G_G(s)G_{R,RT}(s) = \frac{(1.47s+1)}{(0.3s+1)(4.2s+1)(0.08s+1)} \tag{34}$$

Table 1. Controller parameters for Case 1.

Kumar & Anwar [23]	Singh et al. [30]	Sondhi & Hote [22]	Saxena [6]	Güler & Kaya [3]	Proposed CC	
					Internal Loop	External Loop
$K_p = 1.79$	$K_p = 1.50$	$K_p = 2.00$	$K_p = 6.29$	$K_p = 13.36$	$K_{ci} = 14.42$	$K_{co} = 4.69$
$K_i = 3.52$	$K_i = 3.15$	$K_i = 3.00$	$K_{i1} = 15.74$	$K_i = 80.57$	$T_{ii} = 0.30$	$T_{io} = 20.00$
$K_d = 0.30$	$K_d = 0.31$	$\lambda = 0.90$	$K_d = 1.97$	$K_f = 2.67$	$T_{di} = 0.08$	$T_{do} = 0.02$
		$K_d = 0.40$	$K_{i2} = 1.00$	$K_d = 2.93$		
		$\mu = 1.15$	$\lambda = 0.33$			

Table 2. Comparison of performance indices for Case 1. (S.T.: Settling Time, P.V.: Peak Value).

				50% Perturbation					
	Nominal			Upper bound			Lower bound		
DesignMethods	*S.T.* (s)	*P.V.* (10^{-3})	*IAE* (10^{-3})	*S.T.* (s)	*P.V.* (10^{-3})	*IAE* (10^{-3})	*S.T.* (s)	*P.V.* (10^{-3})	*IAE* (10^{-3})
Proposed CC	**0.43**	**1.12**	**0.12**	**2.79**	**1.80**	**0.66**	**1.63**	**0.49**	**0.05**
Güler & Kaya [3]	0.90	2.39	0.40	2.79	3.49	1.17	2.02	1.23	0.18
Saxena [6]	2.24	5.47	2.42	9.69	7.47	12.42	3.28	3.18	1.17
Sondhi & Hote [22]	3.17	6.77	4.29	3.32	9.52	5.98	5.79	3.80	4.26
Singh et al. [30]	1.28	8.56	3.91	5.28	11.77	11.84	3.08	4.87	3.17
Kumar & Anwar [23]	1.56	8.33	3.70	6.83	11.42	13.25	3.14	4.76	2.83

Comparing (34) with (13), one can determine the internal loop's model transfer function parameters as $K_2 = 1$, $T_1 = 1.47$, $T_2 = 0.3$, $T_3 = 4.2$ and $\theta_2 = 0.08$. Similar to the procedure used in case 1, the minimum IAE value is searched to find the values of n and the damping ratio, ξ. The least IAE value of Δf in (29) for the single area PS was reached with $n = 23$ and $\xi = 0.4$. Keeping in mind that $T_s = 0.5s$ is to be used in this work for all case studies, one can evaluate the closed loop time constant is $\tau_c = 0.02$ from (28). Therefore, the internal loop PID controller and filter parameters are obtained as $K_{ci} = 13.82$, $T_{ii} = 0.3$, and $T_{di} = 0.08$ using (16)-(18). The internal loop PID controller filter constants are found to be given by $T_3 = 4.2$ and $T_1 = 1.47$ using expressions provided in Section 3.1. The external loop transfer function, $G_{P1}(s)$, is equal to the load & machine transfer function, $G_P(s)$, of PS with a single area reheat thermal turbine:

$$G_{P1}(s) = G_P(s) = \frac{120}{(20s+1)} \tag{35}$$

Thus, the overall open loop transfer function from (20) is given by:

$$G_t(s) = \frac{120}{(20s+1)(0.02s+1)} \tag{36}$$

By comparing (36) to (20), the external loop's model transfer function parameters $K_1 = 120$,and $T_4 = 20$ are obtained. Then, external loop PID controller and filter parameters values are found as $K_{co} = 4.69$, $T_{io} = 20$ and $T_{do} = 0.02$,and $a = 0.06$ using (23)-(26). The internal and external loop controller parameters of the proposed CC approach and controller parameters of the studies reported in the literature, such as Güler & Kaya [3], Sondhi & Hote [22], Singh et al. [30], Kumar & Anwar [23] and Padhan & Majhi [31], are presented in Table 3. Closed-loop responses of all design methods for $0.01p.u$ load changes at $t = 1s$, are shown in Figure 6a. Responses for all design methods under consideration for +50% and -50% changes in plant transfer function parameters as shown in Figure 6b and Figure 6c, respectively. As in case 1, the proposed CC design

method together with design method Güler & Kaya [3] produce comparable performances in the sense of the least deviation and shortest settling time. Additionally, the proposed approach yields the smoothest response among all design methods. Hence, it may be favourable in practice. Performance assessment indices, in this case, are demonstrated in Table 4 for nominal and ±50% chance in plant transfer function parameters. The table supports the conclusions drawn from the figures.

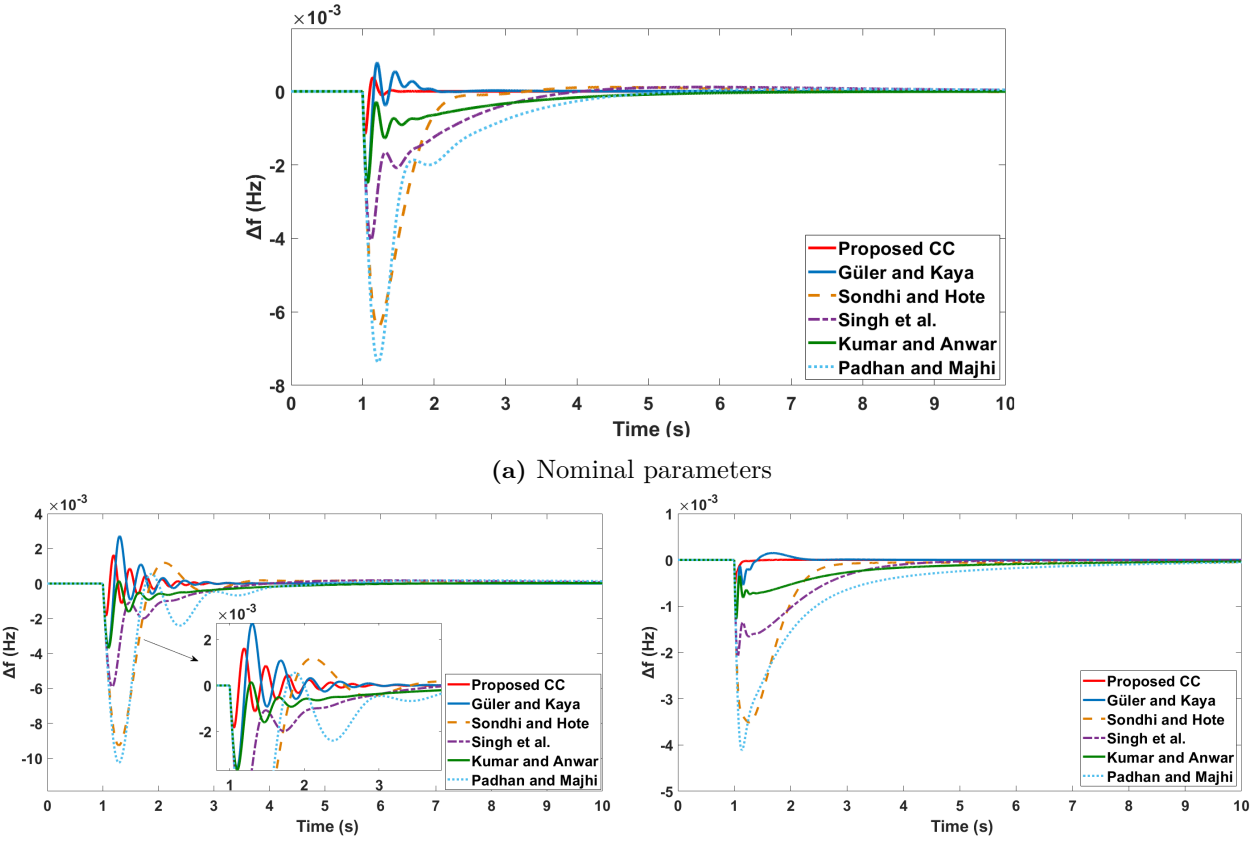

(a) Nominal parameters

(b) +50% perturbations in plant transfer function parameters

(c) -50% perturbations in plant transfer function parameters.

Figure 6. Frequency responses of system for case 2.

4.3. Case 3: LFC design of two-area PS

The block diagram of a two-area PS with a nonreheated thermal turbine is shown in Figure 2. The nominal parameter values of the two-area PS are given in Appendix A.1. In this work, it is assumed that both areas have identical plant transfer functions. Because it is believed that no tie-line power exchange exists, as outlined in Section 2.1, the proposed CC design is carried out with the assumption that each area is independent of the others, and each area's controller design can be performed individually. Following the same procedure as in case 1, the simplified internal loop plant transfer function, $G_{P2}(s)$, is given by (31). Therefore, the internal loop's model transfer function parameters are the same with case 1. In contrast to Case 1, the IAE value of two-area PS must be minimized utilizing (30), which incorporates Δf_1, Δf_2, and ΔP_{tie} to get an enhanced dynamic

response. As a result, the minimum IAE value was achieved with $n = 23$ and $\xi = 0.4$. Remembering that T_s is assumed to be 0.5s, the closed loop time constant is determined to be τ_c, from (28). Thus, using (16)-(18), the internal loop PID controller parameters are found to be $K_{ci} = 13.82$, $T_{ii} = 0.3$ and $T_{di} = 0.08$, as well as the internal loop filter constants $T_1 = 0$ and $T_3 = 0$. The external loop transfer function, $G_{P1}(s)$, is given by (32). Thus, using (20), the overall open-loop transfer function, $G_t(s)$, is as follows:

Table 3. Controller parameters for Case 2.

Padhan & Majhi [31]	Kumar & Anwar [23]	Singh et al. [30]	Sondhi & Hote [22]	Güler & Kaya [3]	Proposed CC	
					Internal Loop	External Loop
$K_p = 6.16$	$K_p = 23.90$	$K_p = 10.25$	$K_p = 6.00$	$K_p = 35.00$	$K_{ci} = 13.82$	$K_{co} = 4.69$
$K_i = 1.93$	$K_i = 5.33$	$K_i = 4.25$	$K_i = 4.00$	$K_i = 196.36$	$T_{ii} = 0.30$	$T_{io} = 20.00$
$K_d = 1.16$	$K_d = 8.11$	$K_d = 3.50$	$\lambda = 0.90$	$K_f = 6.94$	$T_{di} = 0.08$	$T_{do} = 0.02$
			$K_d = 1.00$	$K_d = 7.79$		
			$\mu = 1.20$			

Table 4. Comparison of performance indices for Case 2.

DesignMethods	Nominal			50% Perturbation					
				Upper bound			Lower bound		
	S.T. (s)	*P.V.* (10^{-3})	*IAE* (10^{-3})	*S.T.* (s)	*P.V.* (10^{-3})	*IAE* (10^{-3})	*S.T.* (s)	*P.V.* (10^{-3})	*IAE* (10^{-3})
Proposed CC	**0.42**	**1.15**	**0.12**	**2.82**	**1.85**	**0.7**	**1.44**	**0.50**	**0.04**
Güler & Kaya [3]	0.98	2.48	0.47	2.90	3.62	1.30	2.19	1.27	0.22
Sondhi & Hote [22]	1.34	6.41	4.01	3.26	9.26	6.04	2.74	3.51	3.17
Singh et al. [30]	2.84	4.04	3.38	3.83	5.91	4.19	4.72	2.08	2.34
Kumar & Anwar [23]	4.67	2.50	1.87	5.54	3.69	2.17	7.70	1.26	1.72
Padhan & Majhi [31]	3.65	7.37	5.76	4.73	10.26	7.38	6.87	4.11	4.99

$$G_t(s) = \frac{120}{(20s+1)(0.02s+1)} \tag{37}$$

When (37) is compared to (20), the model transfer function parameters for the external loop are $K_1 = 120$, and $K_4 = 20$. Replacing these values into (23)-(26), the external loop controller and filter parameters $K_{co} = 4.69$, $T_{io} = 20$, $T_{do} = 0.02$, and $a = 0.06$ are identified. Table 5 displays the internal and external controller parameters of the proposed CC design, as well as the controller parameters of alternative design methodologies utilized for comparison. Figure 7 shows the performance of the suggested CC design approach and others used for comparison for $0.01p.u$ load changes in area-1 at $t = 1s$. Figure 7a, Figure 7b, and Figure 7c depict, respectively, the frequency deviation of area-1, the frequency deviation of area-2, and the tie-line power exchange for LFC of two-area PS. As seen in Figure 7, the suggested design technique promptly invalidates frequency variations (Δf_1, Δf_2) and tie-line power exchange (ΔP_{tie}) with almost no overshoots. The area control errors (ACE) of two areas in PS are given in Figure 8, demonstrating the superiority of the proposed CC design method over others used for comparison. Performance evaluation indices provided in Table 6 validates the remarks drawn from Figure 7 and Figure 8.

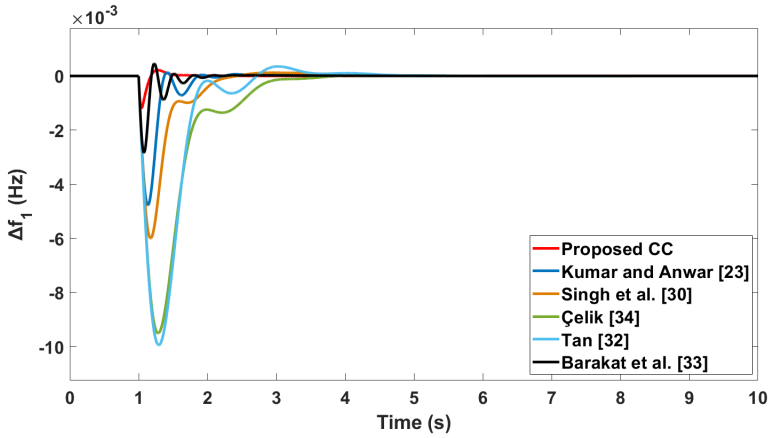

(a) Frequency deviation of area-1

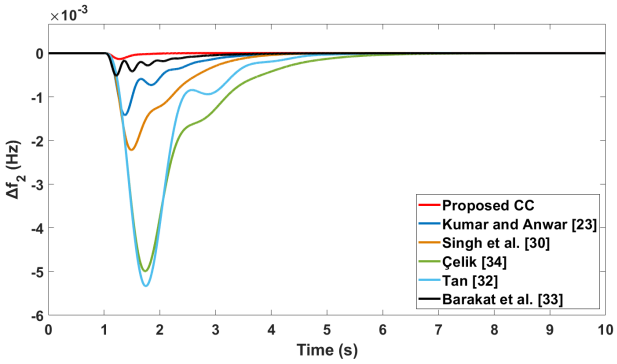

(b) Frequency deviation of area-2

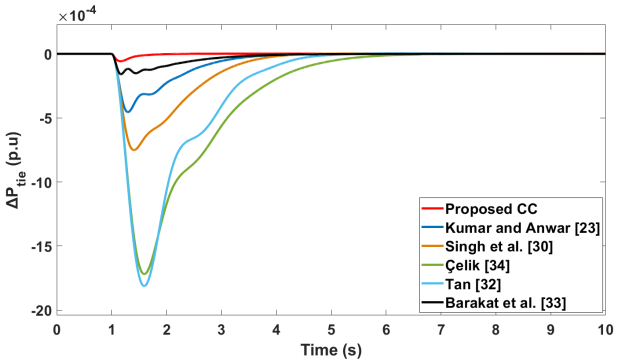

(c) Tie-line power exchange

Figure 7. Responses for Case-3

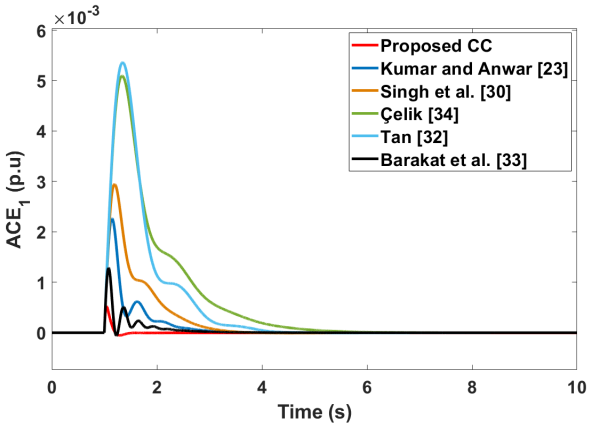

(a) Area-1

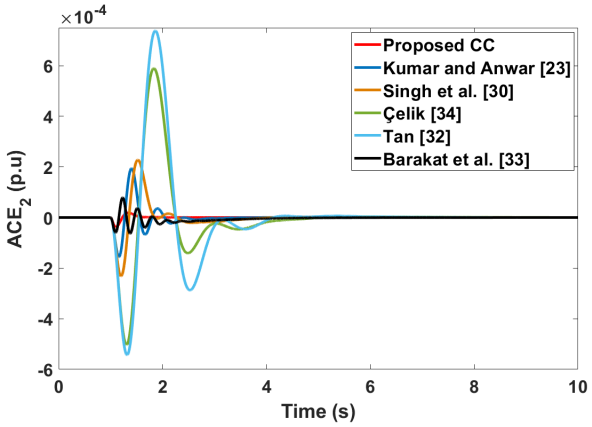

(b) Area-2

Figure 8. Area control errors of PS for Case-3.

Table 5. Controller parameters for Case 3.

Barakat [33]	Tan [32]	Singh et al. [30]	Çelik [34]	Kumar& Anwar[23]	Proposed CC	
					Internal Loop	External Loop
$K_{p1} = 5.00$	$K_p = 1.56$	$K_p = 4.25$	$K_p = 1.62$	$K_p = 8.58$	$K_{ci} = 13.82$	$K_{co} = 4.69$
$K_d = 2.76$	$K_i = 2.39$	$K_i = 5.50$	$K_i = 2.00$	$K_i = 10.88$	$T_{ii} = 0.30$	$T_{io} = 20.00$
$K_{p2} = 1.80$	$K_d = 0.52$	$K_d = 1.35$	$K_d = 0.58$	$K_d = 1.93$	$T_{di} = 0.08$	$T_{do} = 0.02$
$K_i = 5.00$						

Table 6. Comparison of performance indices for Case 3.

Designmethods	Frequency in area-1			Frequency in area-2			Tie-line power		
	S.T. (s)	*P.V.* (10^{-3})	*IAE* (10^{-3})	*S.T.* (s)	*P.V.* (10^{-3})	*IAE* (10^{-3})	*S.T.* (s)	*P.V.* (10^{-4})	*IAE* (10^{-3})
Proposed CC	**0.72**	**1.20**	**0.18**	**1.33**	**0.14**	**0.07**	**1.24**	**0.06**	**0.03**
Barakat[33]	0.96	2.84	0.54	3.04	0.52	0.39	3.78	1.89	0.19
Tan[32]	2.32	9.94	5.51	3.40	5.33	4.92	3.43	18.10	2.10
Singh et al. [30]	2.07	5.99	2.46	2.96	2.21	2.14	3.08	7.51	0.91
Çelik [34]	1.91	9.50	5.91	4.21	4.99	5.88	4.34	17.19	2.50
Kumar & Anwar [23]	0.82	4.77	1.24	2.87	1.41	1.08	3.01	4.55	0.46

4.4. Case 4: Performance of the proposed cascade control design against random load pattern (RLP).

Random step loads at different times, as illustrated in Figure 9, are utilized to verify the robustness of the suggested CC design approach for two-area PS. The RLP in Figure 9 is employed for case 3. The frequency responses of the proposed CC design method against nominal parameters and ±50% parameter changes under different load conditions are illustrated in Figure 11. The performance of the suggested CC system against RLP is depicted in Figure 10 for case-3, demonstrating that the frequency deviations (Δf_1, and Δf_2), and tie-line power exchange (ΔP_{tie}) are within defined limitations. In terms of smoother response without oscillation, faster settling time, and lowest peak value, the suggested CC design method outperforms the examined design methods against RLP. As a result, the proposed CC design approach may be useful in real-time applications since it produces smoother responses with lower deviation and a quicker settling time.

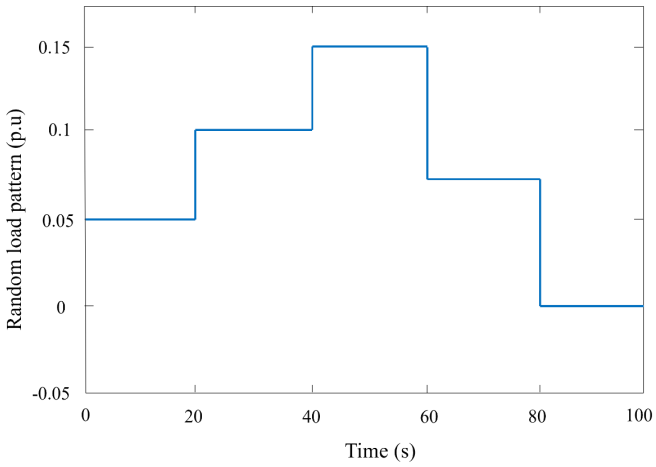

Figure 9. Random load pattern for Case-3.

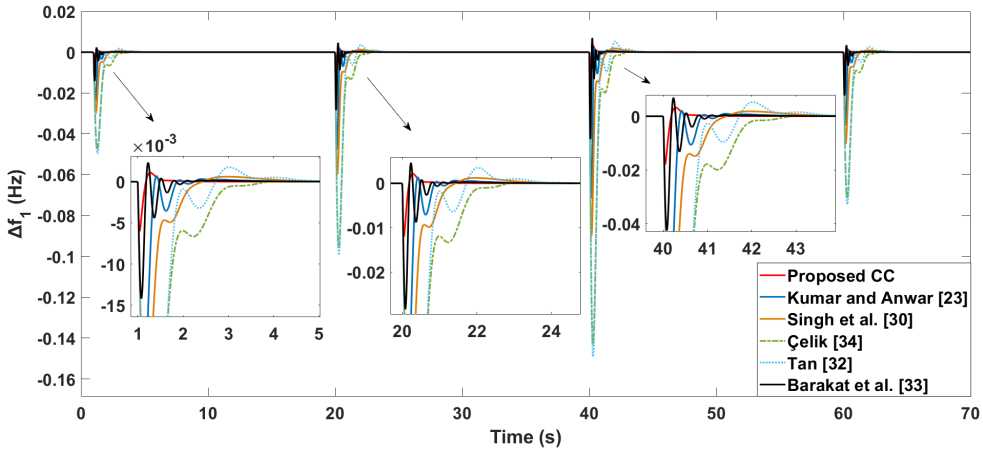

(a) Frequency deviation of area-1.

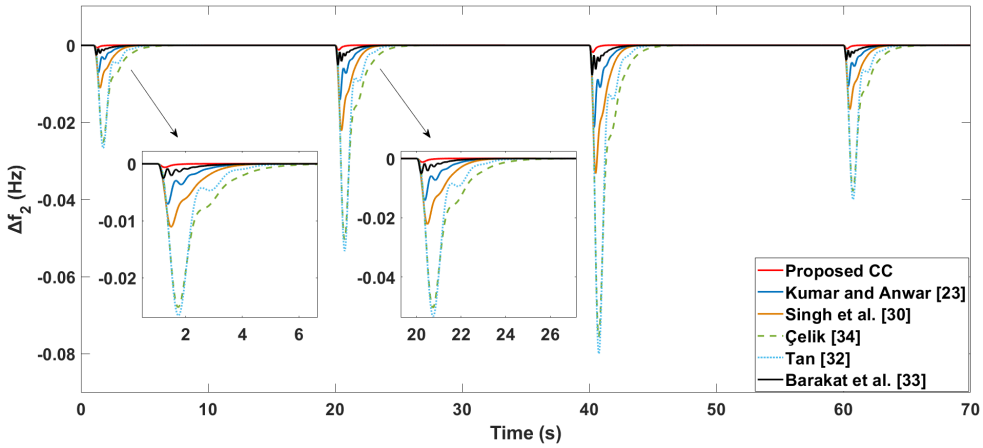

(b) Frequency deviation of area-2.

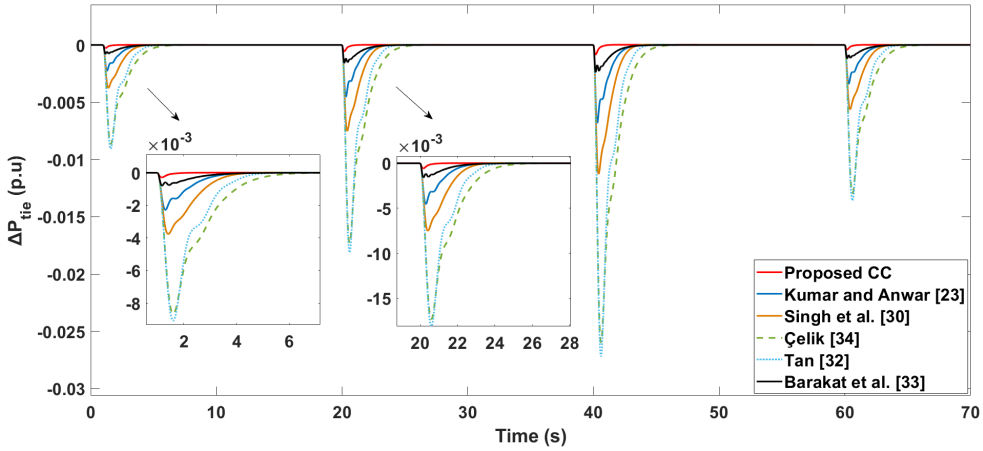

(c) Tie-line power exchange.

Figure 10. Frequency responses and tie-line power exchange against RLP for Case-3.

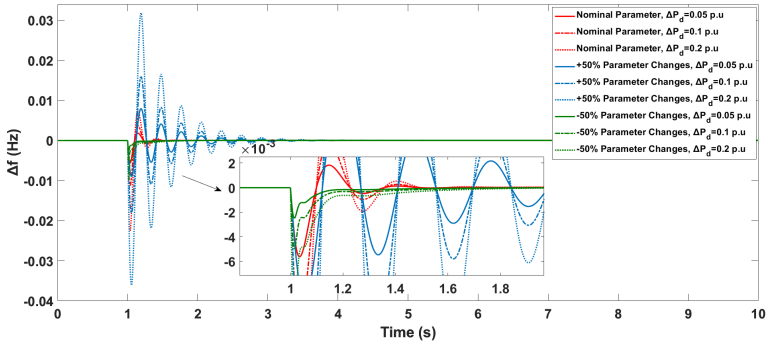

(a) Case-1

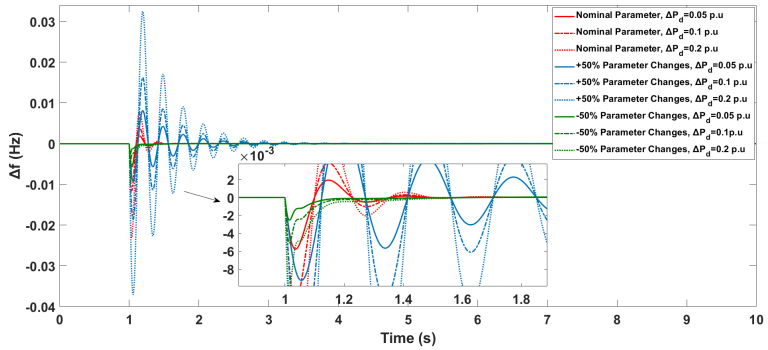

(b) Case-2

Figure 11. The frequency responses depend on nominal parameters and 50% parameter variation under different load conditions in the proposed CC design method.

5. Conclusions

This paper introduces an analytical approach for designing internal and external controllers in a cascade control system, aiming to reduce frequency fluctuations and TLPE of EPS. The controller synthesis approach was employed to identify appropriate controller structures, determined to be serial Proportional-Integral-Derivative controllers with a filter (PIDF) for both loops. This technique is effective in single-area power systems with reheated and nonreheated thermal turbines. The proposed design method was also tested on power systems with two areas. Power systems are tested against load perturbation, variations in plant transfer function parameters, and random load patterns to demonstrate the superiority and robustness of the suggested CC approach. The study compares the proposed CC method with other research in the literature and demonstrates its superiority and robustness. In terms of settling time performances, the proposed CC design method outperforms widely referenced studies in the literature, producing a 52.22% better performance in Case 1. Similarly, in Case 2 and Case 3, the proposed design achieves better performance by 57.14% and 25%, respectively. Power systems are evaluated under different conditions and the proposed CC technique is found to outperform recently published methods in terms of performance and robustness, particularly in single and two-area power systems. Furthermore, the proposed CC design methodology enhances multiarea power system stability by promoting fair tie-line power exchanges, which increases system resilience and protects against sudden system failures caused by unusual fluctuations in any system parameter.

References

[1] Kundur P.Power system stability and control. New York: McGraw Hill; 1994.

[2] Sondhi S, Hote YV. Fractional order PID controller for perturbed load frequency control using Kharitonov's theorem. International Journal of Electrical Power & Energy Systems 2016;78:884–896. https://doi.org/10.1016/j.ijepes.2015.11.103

[3] Güler Y, Kaya I. Load Frequency Control of Single-Area Power System with PI–PD Controller Design for Performance Improvement. Journal Electrical Engineering & Technology 2023;18:2633-2648. https://doi.org/10.1007/s42835-022-01371-1

[4] Dash P, Saikia LC, Sinha N. Flower Pollination Algorithm Optimized PI-PD Cascade Controller in Automatic Generation Control of a Multi-area Power System. International Journal of Electrical Power & Energy Systems 2016; 82: 19–28. https://doi.org/10.1016/j.ijepes.2016.02.028

[5] Padhy S, Panda S. A hybrid stochastic fractal search and pattern search technique based cascade PI-PD controller for automatic generation control of multi-source power systems in presence of plug in electric vehicles. CAAI Transactions on Intelligence Technology 2017; 2 (1): 12–25. https://doi.org/10.1016/j.trit.2017.01.002

[6] Saxena S. Load frequency control strategy via fractional-order controller and reduced-order modeling. International Journal of Electrical Power & Energy Systems 2019; 104: 603–614. https://doi.org/10.1016/j.ijepes.2018.07.005

[7] Sonker B, Kumar D, Samuel P. Dual loop IMC structure for load frequency control issue of multi-area multi-sources power systems. International Journal of Electrical Power & Energy Systems 2019;112:476–494. https://doi.org/10.1016/j.ijepes.2019.04.042

[8] Çelik E, Öztürk N, Arya Y, Ocak C. (1 + PD)-PID cascade controller design for performance betterment of load frequency control in diverse electric power systems. Neural Computing Applications 2021;33:15433–15456. https://doi.org/10.1007/s00521-021-06168-3

[9] Kumar A, Anwar MN, Kumar S. Sliding mode controller design for frequency regulation in an interconnected power system. Protection and Control Modern Power Systems 2021; 6:6. https://doi.org/10.1186/s41601-021-00183-1

[10] Kumar A, Anwar MN, Huba M. Load Frequency Controller Design Based on the Direct Synthesis Approach Using a 2DoF-IMC Scheme for a Multi-Area Power System. Symmetry 2022;14 (10):1994. https://doi.org/10.3390/sym14101994

[11] Saka M, Sönmez Ş, Eke İ, Gözde H, Taplamacıoğlu MC et al. Inserting of heuristic techniques into the stability regions for multiarea load frequency control systems with time delays. Turkish Journal of Electrical Engineering and Computer Sciences 2022;30 (6):2286–2302. https://doi.org/10.55730/1300-0632.3939

[12] Barakat M, Mabrouk AM, Donkol A. Optimal design of a cascade controller for frequency stability of photovoltaic–reheat thermal power systems considering nonlinearities. Optical and Quantum Electronics 2023;55:295. https://doi.org/10.1007/s11082-023-04583-5

[13] Abou El-Ela AA, El-Sehiemy RA, Shaheen AM, Diab AE-G. Design of cascaded controller based on coyote optimizer for load frequency control in multi-area power systems with renewable sources. Control Engineering Practice 2022121:105058. https://doi.org/10.1016/j.conengprac.2021.105058

[14] Choudhary R, Rai JN, Arya Y. Cascade FOPI-FOPTID controller with energy storage devices for AGC performance advancement of electric power systems. Sustainable Energy Technologies and Assessments 2022;53:102671. https://doi.org/10.1016/j.seta.2022.102671

[15] Khokhar B, Dahiya S, Parmar KPS. A novel fractional order proportional integral derivative plus second-order derivative controller for load frequency control. International Journal of Sustainable Energy 2021;40 (3):235–252. https://doi.org/10.1080/14786451.2020.1803861

[16] Çelik E. Performance analysis of SSA optimized fuzzy 1PD-PI controller on AGC of renewable energy assisted thermal and hydro-thermal power systems. Journal of Ambient Intelligence and Humanized Computing 2022;13:4103–4122. https://doi.org/10.1007/s12652-022-03751-x

[17] Khokhar B, Dahiya S, Singh Parmar KP. A Robust Cascade Controller for Load Frequency Control of a Standalone Microgrid Incorporating Electric Vehicles. Electric Power Components and Systems 2020;48:711–726. https://doi.org/10.1080/15325008.2020.1797936

[18] Khokhar B, Dahiya S, Parmar KPS. A Novel Hybrid Fuzzy PD-TID Controller for Load Frequency Control of a Standalone Microgrid. Arabian Journal for Science and Engineering 2021;46:1053–1065. https://doi.org/10.1007/s13369-020-04761-7

[19] Çelik E. Design of new fractional order PI–fractional order PD cascade controller through dragonfly search algorithm for advanced load frequency control of power systems. Soft Computing 2021;25:1193–1217. https://doi.org/10.1007/s00500-020-05215-w

[20] Kaya I. Improving performance using cascade control and a Smith predictor. ISA Transactions 2001;40 (3):223–234. https://doi.org/10.1016/S0019-0578(00)00054-9

[21] Sharma J, Hote YV, Prasad R. PID controller design for interval load frequency control system with communication time delay. Control Engineering Practice 2019;89:154–168. https://doi.org/10.1016/j.conengprac.2019.05.016

[22] Sondhi S, Hote YV. Fractional order PID controller for load frequency control. Energy Conversion and Management 2014;85:343–353. https://doi.org/10.1016/j.enconman.2014.05.091

[23] Kumar A, Anwar MN. Decentralized Load–Frequency Controller Design for a Single as Well as Multi-area Power System. Iranian Journal of Science and Technology, Transactions of Electrical Engineering 2020;44:309–326. https://doi.org/10.1007/s40998-019-00246-y

[24] Anwar MN, Pan S. A new PID load frequency controller design method in frequency domain through direct synthesis approach. International Journal of Electrical Power & Energy Systems 2015;67:560–569. https://doi.org/10.1016/j.ijepes.2014.12.024

[25] Kaya İ, Tan N, Atherton DP. Improved cascade control structure for enhanced performance. Journal of Process Control 2007;17 (1):3–16. https://doi.org/10.1016/j.jprocont.2006.08.008

[26] Arya Y, Dahiya P, Çelik E, Sharma G, Gözde H et al. AGC performance amelioration in multi-area interconnected thermal and thermal-hydro-gas power systems using a novel controller. Engineering Science and Technology, an International Journal 2021;24 (2):384–396. https://doi.org/10.1016/j.jestch.2020.08.015

[27] Kaya İ, Nalbantoğlu M. Simultaneous tuning of cascaded controller design using genetic algorithm. Electrical Engineering 2016;98:299–305. https://doi.org/10.1007/s00202-016-0367-4

[28] Kaya I, Nalbantoglu M. Cascade controller design using controller synthesis. IEEE 2015 19th International Conference on System Theory, Control and Computing; Cheile Gradistei, Romania; 2015, p. 32–36. https://doi.org/10.1109/ICSTCC.2015.7321265

[29] Kaya I. Obtaining controller parameters for a new PI-PD Smith predictor using autotuning. Journal of Process Control 2003;13 (5):465–472. https://doi.org/10.1016/S0959-1524(02)00086-0

[30] Singh VP, Kishor N, Samuel P. Improved load frequency control of power system using LMI based PID approach. Journal of the Franklin Institute 2017;354 (15): 6805–6830. https://doi.org/10.1016/j.jfranklin.2017.08.031

[31] Padhan DG, Majhi S. A new control scheme for PID load frequency controller of single-area and multi-area power systems. ISA Transactions 2013;52 (2):242–251. https://doi.org/10.1016/j.isatra.2012.10.003

[32] Wen Tan. Unified Tuning of PID Load Frequency Controller for Power Systems via IMC. IEEE Transactions on Power Systems 2010;25 (1):341–350. https://doi.org/10.1109/TPWRS.2009.2036463

[33] Barakat M, Donkol A, Hamed HFA, Salama GM. Harris Hawks-Based Optimization Algorithm for Automatic LFC of the Interconnected Power System Using PD-PI Cascade Control. Journal of Electrical Engineering & Technology 2021;16:1845–1865. https://doi.org/10.1007/s42835-021-00729-1

[34] Çelik E. Improved stochastic fractal search algorithm and modified cost function for automatic generation control of interconnected electric power systems. Engineering Applications of Artificial Intelligence 2020;88:103407. https://doi.org/10.1016/j.engappai.2019.103407

[35] Saxena S, Biradar S. Fractional-order IMC controller for high-order system using reduced-order modelling via Big-Bang, Big-Crunch optimisation. International Journal of Systems Science 2022;53 (1):168–181. https://doi.org/10.1080/00207721.2021.1942587

Appendix A

A.1 Nominal parameters of the two-area PS: $f = 60Hz, K_{Pi} = 120Hz/p.u, T_{Pi} = 20s, T_{Ti} = 0.3s, T_{Gi} = 0.08s$, $R_i = 2.4Hz/p.u, B_i = 0.425p.u.MW/Hz, T_{12} = 0.0866p.u.MW/rad$. [19, 23, 30, 32, 33]

Table 7. Nomenclature

Δf_i: Incremental change in the area frequency	B_i: Frequency response characteristics
T_G: Governor time constant	ΔP_{tiei}: Tie-line power error
T_{Ti}: Turbine time constant	α_{12},α_{13},α_{23}: Area size ratio
T_{Ri}: Constant of reheat turbine	T_{12},T_{13},T_{23}: Tie-line synchronizing coefficient
c: Percentage of power generated in the reheat portion	ACE_i: Area control error
K_{Pi}: Electric system gain	ΔP_{Di}: Load disturbance
T_{Pi}: Electric system time constant	ΔP_{ti}: Incremental change in generator output
ΔP_{gi}: Incremental change in governor valve position	u_i: Controller output
R_i: Speed regulation due to governor action	i: Subscript referring to area- i ($i = 1, 2$)
K_r: Reheat turbine gain	ΔP_{tiei-j}: Incremental change in tie line power connecting between area i and area j (p.u.)